The Astrophysical Journal, 806:230 (9pp), 2015 June 20 doi:10.1088/0004-637X/806/2/230

A DEEP STUDY OF THE DWARF SATELLITES ANDROMEDA XXVIII AND ANDROMEDA XXIX

Colin T. Slater[1], Eric F. Bell[1], Nicolas F. Martin[2], Erik J. Tollerud[3], and Nhung Ho[3]
[1] Department of Astronomy, University of Michigan, 1085 S. University Ave., Ann Arbor, MI 48109, USA
[2] Observatoire astronomique de Strasbourg, Université de Strasbourg, CNRS, UMR 7550, 11 rue de l'Université, F-67000 Strasbourg, France
[3] Astronomy Department, Yale University, P.O. Box 208101, New Haven, CT 06510, USA
Received 2014 October 26; accepted 2015 May 7; published 2015 June 19

ABSTRACT

We present the results of a deep study of the isolated dwarf galaxies Andromeda XXVIII and Andromeda XXIX with Gemini/GMOS and Keck/DEIMOS. Both galaxies are shown to host old, metal-poor stellar populations with no detectable recent star formation, conclusively identifying both of them as dwarf spheroidal galaxies (dSphs). And XXVIII exhibits a complex horizontal branch morphology, which is suggestive of metallicity enrichment and thus an extended period of star formation in the past. Decomposing the horizontal branch into blue (metal-poor, assumed to be older) and red (relatively more metal-rich, assumed to be younger) populations shows that the metal-rich are also more spatially concentrated in the center of the galaxy. We use spectroscopic measurements of the calcium triplet, combined with the improved precision of the Gemini photometry, to measure the metallicity of the galaxies, confirming the metallicity spread and showing that they both lie on the luminosity–metallicity relation for dwarf satellites. Taken together, the galaxies exhibit largely typical properties for dSphs despite their significant distances from M31. These dwarfs thus place particularly significant constraints on models of dSph formation involving environmental processes such as tidal or ram pressure stripping. Such models must be able to completely transform the two galaxies into dSphs in no more than two pericentric passages around M31, while maintaining a significant stellar population gradient. Reproducing these features is a prime requirement for models of dSph formation to demonstrate not just the plausibility of environmental transformation but the capability of accurately recreating real dSphs.

Key words: galaxies: dwarf – galaxies: individual (And XXVIII – And XXIX) – Local Group

1. INTRODUCTION

The unique physical properties and environments of dwarf galaxies make them excellent test cases for improving our understanding of the processes that affect the structure, stellar populations, and evolution of galaxies. Because of their shallow potential wells, dwarf galaxies are particularly sensitive to a wide range of processes that may only weakly affect larger galaxies. These processes range from cosmological scales, such as heating by the UV background radiation (Gnedin 2000), to interactions at galaxy scales such as tidal stripping and tidal stirring (Mayer et al. 2001; Kravtsov et al. 2004; Klimentowski et al. 2009), resonant stripping (D'Onghia et al. 2009), and ram pressure stripping (Mayer et al. 2006), to the effects of feedback from from the dwarfs themselves (Dekel & Silk 1986; Mac Low & Ferrara 1999; Gnedin & Zhao 2002; Sawala et al. 2010).

Many studies have focused on understanding the differences between the gas-rich, star forming dwarf irregular galaxies (dIrrs) and the gas-poor, non-star-forming dwarf spheroidals. While a number of processes could suitably recreate the broad properties of this differentiation, finding observational evidence in support of any specific theory has been difficult. One of the main clues in this effort is the spatial distribution of dwarfs; while dIrrs can be found throughout the Local Group, dwarf spheroidal galaxies (dSphs) principally are only found within 200–300 kpc of a larger host galaxy such as the Milky Way or Andromeda (Einasto et al. 1974; van den Bergh 1994; Grebel et al. 2003). This is trend is also reflected in the gas content of Local Group dwarfs (Blitz & Robishaw 2000; Grcevich & Putman 2009). This spatial dependence seems to indicate that environmental effects such as tides and ram pressure stripping are likely to be responsible for creating dSphs. However, there are outliers from this trend, such as Cetus, Tucana, and Andromeda XV, which are dSphs that lie more than 700 kpc from either the Milky Way or Andromeda. The existence of such distant dSphs may suggest that alternative channels for dSph formation exist (Kazantzidis et al. 2011b), or it could be an incidental effect seen in galaxies that have passed through a larger host on very radial orbits (Teyssier et al. 2012; Slater & Bell 2013).

The set of isolated dwarf galaxies was recently enlarged by the discovery of Andromeda XXVIII and XXIX, which by their position on the sky were known to be approximately 360 and 200 kpc from Andromeda, respectively (Bell et al. 2011; Slater et al. 2011). While And XXIX was identified as a dSph by the images confirming it as a galaxy, there was no comparable data on And XXVIII (beyond the initial Sloan Digital Sky Survey (SDSS) discovery data) with which to identify it as a dSph or dIrr. We thus sought to obtain deeper imaging of both galaxies down to the horizontal branch level which would enable a conclusive identification of the galaxies as dSphs or dIrrs by constraining any possible recent star formation. In addition, the deep photometry permits more precise determination of the spatial structure and enables the interpretation of the spectroscopic calcium triplet data from Tollerud et al. (2013) to obtain a metallicity measurement. As we will discuss, the information derived from these measurements along with dynamical considerations imposed by their position in the Local Group can together place significant constraints on plausible mechanisms for the origin of these two dSphs.

This work is organized as follows: we discuss the imaging data and the reduction process in Section 2, and illustrate the general features of the color–magnitude diagram in Section 3. Spectroscopic metallicities are presented in Section 4, and the

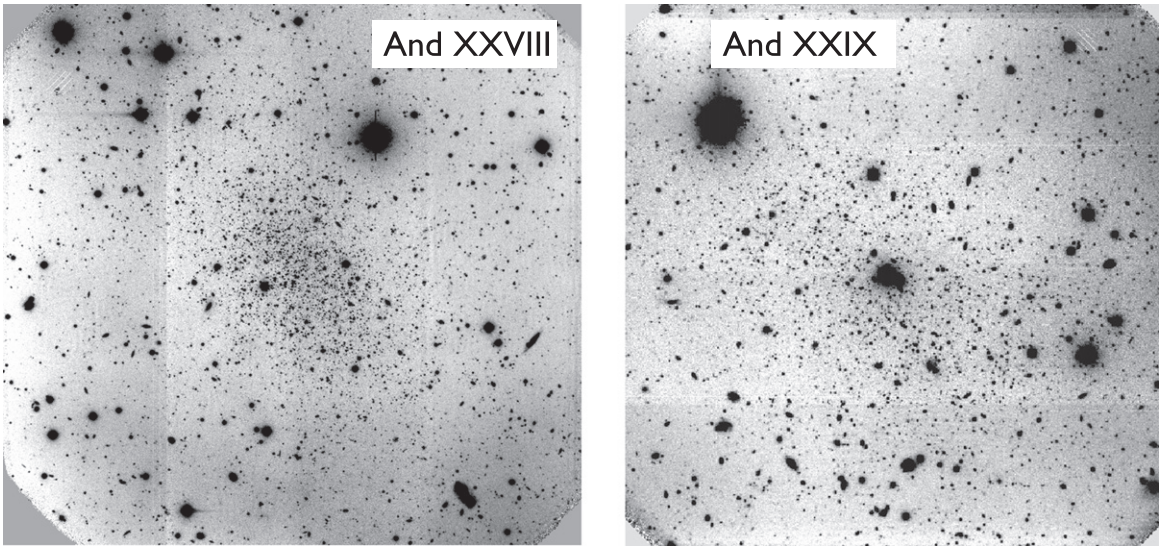

Figure 1. Stacked *i*-band image of And XXVIII on the left, and of And XXIX on the right. North is up, and east is to the left. Both images are approximately 5.′6 on a side. The saturated feature near the center of And XXIX is a combination of a foreground star and two background galaxies.

structure and stellar populations of the dwarfs are discussed in Section 5. We discuss the implications of these results for theories of dSph formation in Section 6.

2. IMAGING OBSERVATIONS AND DATA REDUCTION

Between 2012 July 22 and August 13 we obtained deep images of And XXVIII and XXIX with the GMOS instrument on Gemini-North (Gemini program GN-2012B-Q-40). The observations for each dwarf consisted of a total of 3150 s in SDSS-*i* band and 2925 s in *r*, centered on the dwarf. Because the dwarfs each nearly fill the field of view (FOV) of the instrument, we also obtained a pair of flanking exposures for each dwarf to provide an "off-source" region for estimating the contamination from background sources. These exposures consisted of at least 1350 s in both *r* and *i*, though some fields received a small number of extra exposures. The images were all taken in 70th percentile image quality conditions or better, which yielded excellent results with the point source FWHM ranging between 0.″47 and 0.″8.

All of the images were bias subtracted, flat fielded, and coadded using the standard bias frames and twilight flats provided by Gemini. The reduced images can be seen in Figure 1. Residual flat fielding and/or background subtraction uncertainty exists at the 1% level (0.01 magnitudes, roughly peak to valley). Point-spread function (PSF) photometry was performed using DAOPHOT (Stetson 1987), which enabled accurate measurements even in the somewhat crowded centers of the dwarfs. In many cases the seeing in one filter was much better than the other, such as for the core of And XXVIII where the seeing was 0.″47 in *i* and 0.″68 in *r*. In these cases we chose to first detect and measure the position of stars in the image with the best seeing, and then require the photometry of the other band to reuse the positions of stars detected in the better band. This significantly extends our detection limit, which would otherwise be set by the shallower band, but with limited color information at these faint magnitudes.

The images were calibrated to measurements from the SDSS, Data Release 9 (Ahn et al. 2012). For each stacked image we cross-matched all objects from the SDSS catalog that overlapped our fields, with colors between $-0.2 < (r - i)_0 < 0.6$, and classified as stars both by SDSS and DAOPHOT. Star-galaxy separation was performed using the "sharp" parameter from DAOPHOT. From this we measured the weighted mean offset between the SDSS magnitudes and the instrumental magnitudes to determine the zeropoint for each field. Between the saturation limit of the Gemini data, mitigated by taking several exposures, and faint limits of the SDSS data (corresponding to approximately $19 < i < 22.5$ and $19.5 < r < 22.5$) there were of the order of 100 stars used for the calibration of each frame. Based on the calculated stellar measurement uncertainties the formal uncertainty on the calibration is at the millimagnitude level, but unaccounted systematic effects likely dominate the statistical uncertainty (e.g., precision reddening measurements). All magnitudes were dereddened with the extinction values from Schlafly & Finkbeiner (2011).

The photometric completeness of each stacked image was estimated by artificial star tests. For each field we took the PSF used by DAOPHOT for that field and inserted a large grid of artificial stars, with all of the stars at the same magnitude but with Poisson noise on the actual pixel values added to each image. This was performed for both *r* and *i* band images simultaneously, and the resulting pair of images was then run through the same automated DAOPHOT pipeline that was used on the original image. Artificial stars were inserted over a grid of *i* band magnitudes and $r - i$ colors, producing measurements of the recovery rate that cover the entire CMD. The 50% completeness limit for both dwarfs is at least $r_0 = 25.5$, with slightly deeper data in the *i*-band for And XXVIII.

The observed CMDs suffer from both foreground and background contamination. Foreground dwarf stars in the Milky Way tend to contribute at the bright end of the CMD. At the faint end, distant galaxies that are too small to be resolved become the dominant source of contamination. This effect can quickly become significant at fainter magnitudes due to the rapid rise in the observed galaxy luminosity function. This effect was minimized by the superb seeing at the Gemini observatory, which allowed smaller galaxies to be resolved and excluded from our sample.

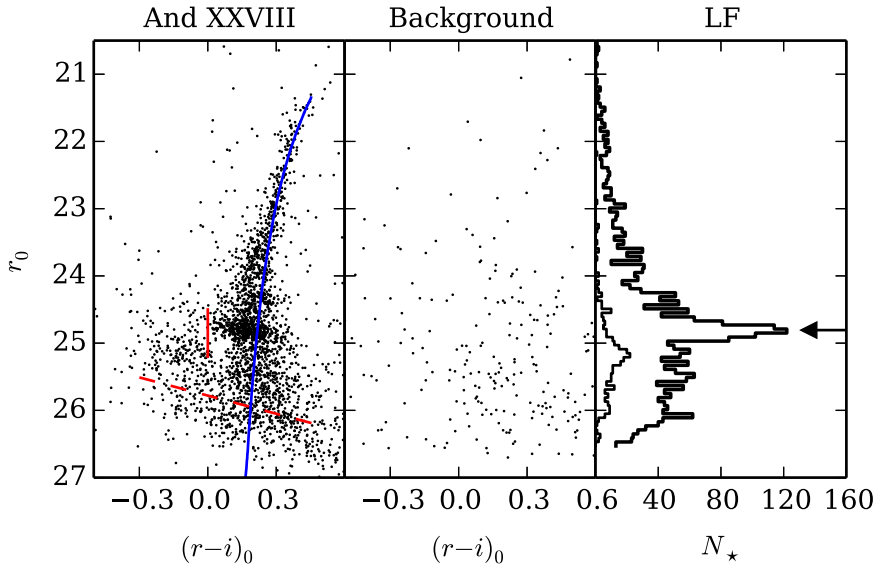

Figure 2. CMD of And XXVIII on the left (inside $2r_h$), with the CMD of an equal-sized background region in the center. The red dashed line indicates the 50% completeness limit, while the vertical red line indicates the approximate division between red and blue horizontal branches. The luminosity function of the dwarf is shown on the right, separated into a thick line showing stars with $(r-i)_0 > 0$ and a thin line showing stars with $(r-i)_0 < 0$. A 12 Gyr old, [Fe/H] = −1.84 isochrone is overplotted, and the measured apparent magnitude of the HB is indicated with an arrow.

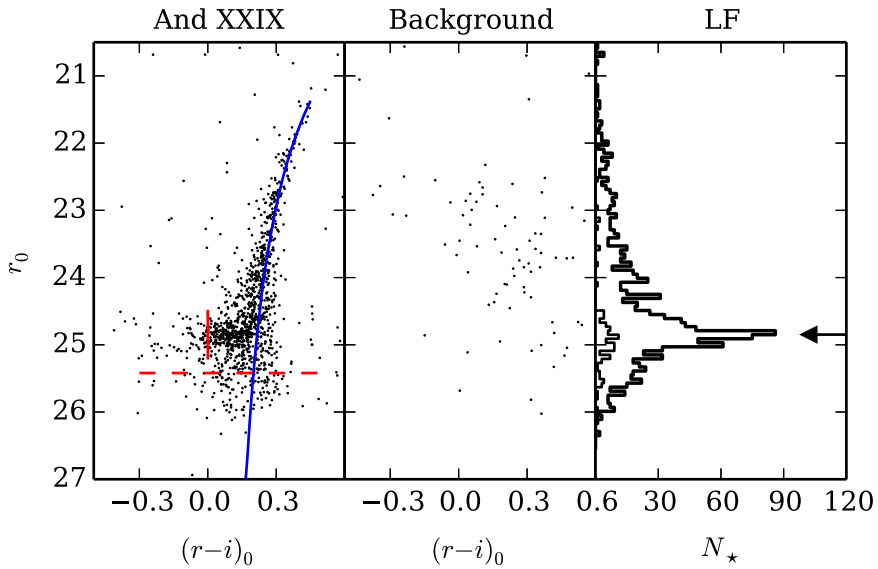

Figure 3. Same panels as Figure 2, but for And XXIX. A 12 Gyr old, [Fe/H] = −1.92 isochrone is overplotted. As with And XXVIII there are no indications of recent star formation. Though there may be some hints of a BHB, if it does exist it is substantially less prominent than in And XXVIII.

3. OBSERVED CMDS

The CMDs of And XXVIII and XXIX are shown in the left panels of Figures 2 and 3, respectively. A 12 Gyr old isochrone from Dotter et al. (2008) is overlaid at the distances and spectroscopic metallicities determined later in this work. Both dwarfs show a well-populated giant branch with a very prominent red clump/red horizontal branch (RC/RHB) near $r_0 \sim 24.5$–25.0. This feature is particularly clear as a large bump in the luminosity functions of each dwarf, shown by the thick black line in the right panels of Figures 2 and 3. In addition to the RC/RHB, And XXVIII also shows a blue horizontal branch (BHB) slightly fainter than $r_0 \sim 25.0$ and spanning $-0.3 < (r-i)_0 < 0.0$ in color. The luminosity function for stars with $(r-i)_0 < 0.0$ is shown by the thin line on the right panel of Figure 2. The presence of a complex horizontal branch suggests that And XXVIII has had an extended star formation history, since the BHB is typically seen in the oldest globular clusters, while the RHB tends to appear in globular clusters roughly 2–4 Gyr younger than the oldest populations (Stetson et al. 1989; Sarajedini et al. 1995), although a few globular clusters do show both BHB and RHB (An et al. 2008). The additional information from the spectroscopic metallicity spread, as will be discussed below, also confirms the extended star formation in both dwarfs. And XXIX does not show the same prominent BHB. There are 5–10 stars in a similar position as the BHB in And XXVIII, but this is almost negligible compared to the 100 or more stars in the BHB of And XXVIII and could be background contamination. This does not indicate that there is no ancient population in And XXIX, as, for example, the Draco dSph also contains very few BHB stars (Ségall et al. 2007).

There is a notable absence of any young main-sequence stars in the observed CMDs of both XXVIII and XXIX, which suggests that there has not been any recent star formation at appreciable rates in either galaxy. The handful of stars brighter than the HB and on the blue side of the RGB are consistent with foreground (or background) contamination. The CMD of And XXIX has an almost negligible number of stars bluewards of the RGB at any magnitude. The CMD of And XXVIII does show some blue detections below the BHB, but it is difficult to conclusively identify their origin. Since the precision of the colors degrades at faint magnitudes, these detections could be an (artificial) broadening of the RGB, possibly scattering more stars toward the blue due to the somewhat shallower depth of the *r*-band exposures. It is also possible that they are background sources or false detections from noise, both of which could be strongly weighted toward the faintest magnitudes. None of these origins are clearly favored and some combination could be at work, but there is not sufficient evidence to believe that these sources are main sequence stars.

The absence of observed young main sequence stars in And XXVIII is complemented by recent work that shows little to no cold gas in the galaxy. Observations with the Westerbork Synthesis Radio Telescope place a $5-\sigma$ upper limit on the total HI mass of $2.8 \times 10^3\,M_\odot$ (T. Oosterloo 2015, private communication). For comparison, the similarly low-mass dwarf Leo T has had recent star formation and contains $\sim 2.8 \times 10^5\,M_\odot$ of HI (Ryan-Weber et al. 2008), while most dSphs have upper limits at this level or less (Grcevich & Putman 2009). This stringent limit on the gas in And XXVIII adds further evidence that it is a dSph.

3.1. Distance and Luminosity

The clear HB in both dwarfs enables an accurate measurement of the distance to the dwarfs, and hence their distance to M31. We fit a Gaussian plus a linear background model to the *r*-band luminosity function of each dwarf in the region of the HB, using only stars redder than $(r-i)_0 = 0$. The measured HB position is indicated in the right panels of Figures 2 and 3 by the horizontal arrow, and is $m_{g,0} = 24.81$ for And XXVIII and $m_{g,0} = 24.84$ for And XXIX. We use the RHB absolute magnitude calibration of Chen et al. (2009), which is based on globular cluster RHBs measured directly in the SDSS filter set. In the *r*-band this calibration, using a linear metallicity dependence and without the age term, is

$$M_r = 0.165\,[\mathrm{Fe/H}] + 0.569. \quad (1)$$

The resulting distances are 811 ± 48 kpc for And XXVIII and 829 ± 42 kpc for And XXIX, using the spectroscopic metallicities as determined in Section 4. Both of these are slightly farther than the measured distances from Slater et al. (2011) and Bell et al. (2011), but just within (And XXVIII) or just outside (And XXIX) the formal one-sigma uncertainties. The updated heliocentric distances does not substantially change the measured distances between the dwarfs and M31, since both are near the tangent point relative to M31.[4] Based on these distances, both dwarfs lie well away from the plane of satellites from Conn et al. (2013) and Ibata et al. (2013). As seen from M31 the satellites are 80° (And XXVIII) and 60° (And XXIX) from the plane. The closest galaxy to And XXVIII is And XXXI at 164 kpc, while And XXIX's closest neighbor is And XIX at 88 kpc, making both relatively isolated from other dwarfs.

[4] The distance between And XXIX and M31 reported in Bell et al. (2011) was incorrect due to a geometry error; it is fixed in this work.

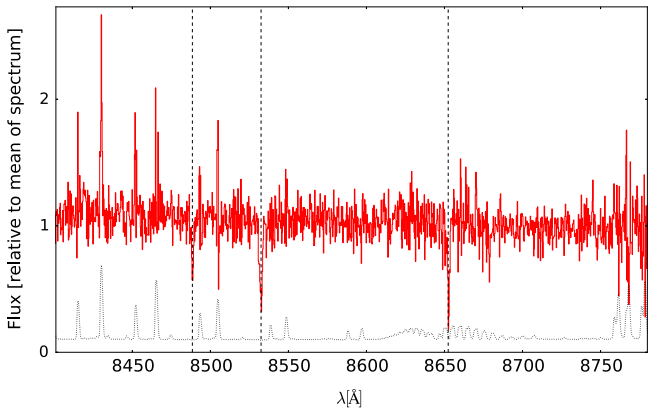

Figure 4. Example spectrum of an individual star in And XXVIII, focusing on the triplet of calcium lines (marked with vertical dashed lines, and shifted to the velocity of And XXVIII). The dotted line indicates the rms uncertainty at each point in the spectrum.

We measured the total luminosity of both dwarfs by comparing the portion of the LF brighter than the HB to the LF of the Draco dwarf. Using data from Ségall et al. (2007) we constructed a background-subtracted LF for Draco inside r_h, then scaled the LF of the dwarfs such that they best matched the Draco LF. The resulting luminosities are $M_V = -8.7 \pm 0.4$ for And XXVIII and $M_V = -8.5 \pm 0.3$ for And XXIX, both of which are again in good agreement with values measured by previous works.

4. SPECTROSCOPIC METALLICITY

To complement the imaging data, we also make use of metallicities derived from Keck/DEIMOS spectroscopy of the brightest RGB stars. The source data and spectroscopic reductions are described in Tollerud et al. (2013), and a sample spectrum is shown in Figure 4. We derive metallicities from the $\lambda \sim 8550$ Å calcium triplet features, following the methodology described in Ho et al. (2015). Briefly, this procedure fits a Gaussian profile to the strongest two CaT lines, and uses these fits to derive CaT equivalent widths. In combination with absolute magnitudes from the aforementioned photometric data (Section 2), these data can be calibrated to act as effective proxies for [Fe/H] of these stars. For this purpose, we adopt the Carrera et al. (2013) metallicity calibration to convert our photometry and equivalent widths to [Fe/H].

A table of the spectroscopic metallicity measurements of individual stars in each dwarf is presented in Table 2. We determine the uncertainty in the galaxy mean [Fe/H] by performing 1000 Monte Carlo resamplings of the distribution. For each resampling, we add a random offset to the metallicity of each star drawn from a Gaussian with width of the per-star [Fe/H] uncertainty, and compute the mean of the resulting distribution. For measuring each galaxy's metallicity spread σ ([Fe/H]), we report the second moment of the individual measurement distribution and derive uncertainties from a resampling procedure like that for the galaxy mean [Fe/H].

The resulting metallicity distributions for And XXVIII and XXIX are shown as cumulative distribution functions in Figure 5. From this it is immediately clear that, while the

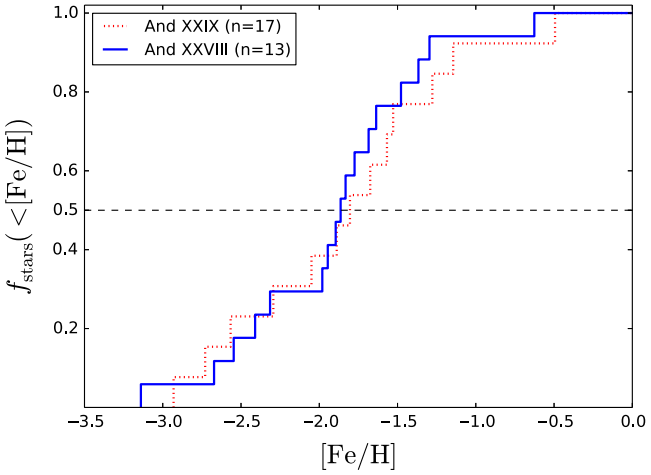

Figure 5. Cumulative distribution of [Fe/H] for And XXVIII (blue solid line) and XXIX (red dotted line).

number of stars is relatively small, the median of the distribution peaks at [Fe/H] ~ -2 (see Table 1). Motivated by this, in Figure 6, we show the luminosity–metallicity relation for the brighter M31 satellites (Ho et al. 2015) and the MW satellites (Kirby et al. 2011, 2013), using luminosities from N. F. Martin et al. (2015, in preparation). It is immediately clear from this figure that And XXVIII and XXIX are fully consistent with the metallicity–luminosity relation that holds for other Local Group satellites. Our measurement for And XXVIII is also consistent with the prior measurement by Collins et al. (2013) of [Fe/H] $= -2.1 \pm 0.3$, but at higher precision.

5. STRUCTURE AND STELLAR POPULATIONS

We determined the structural properties of the dwarfs using an updated version of the maximum likelihood method presented in Martin et al. (2008). This method fits an exponential radial density profile to the galaxies without requiring the data to be binned, which enables more precise measurements of the structure in galaxies with only a small number of observed stars. The updated version samples the parameter space with a Markov Chain Monte Carlo process, and can more easily account for missing data (N. F. Martin et al. 2015, in preparation). This is necessary to account for the limited FOV of GMOS, which could cause a systematic size error (Muñoz et al. 2012), as well as the very center of And XXIX where an inconveniently located bright foreground star contaminates the very center of the image and prevents reliable photometry in the surrounding region.

The resulting radial profiles and posterior probability distributions are shown in Figures 7 and 8. The half-light radii and ellipticities all have fairly typical values for other dwarfs of similar luminosities (Brasseur et al. 2011). The results are also consistent with the parameters estimated from the much shallower SDSS data (Bell et al. 2011; Slater et al. 2011).

The separation between the red and blue horizontal branches in And XXVIII enables us to examine the spatial distribution of the metal-poor, older, and the more metal-rich, younger, stellar populations. Radial profiles of the two horizontal branches (separated at $(r-i)_0 = 0.0$) are shown in Figure 9. The difference in the radial profiles is easily seen in the right panel,

Table 1
Properties of And XXVIII and XXIX

Parameter	And XXVIII	And XXIX
α(J2000)	$22^{\rm h}32^{\rm m}41\overset{\rm s}{.}5$	$23^{\rm h}58^{\rm m}55\overset{\rm s}{.}6$
δ (J2000)	31° 13′ 3.″7	30° 45′ 20.″2
$E(B-V)$	0.080[a]	0.040[a]
Ellipticity	0.43 ± 0.02	0.29 ± 0.04
Position Angle (N to E)	$34° \pm 1°$	$55° \pm 4°$
r_h	$1\overset{'}{.}20 \pm 0\overset{'}{.}03$	$1\overset{'}{.}39 \pm 0\overset{'}{.}08$
r_h	280 ± 20 pc	315 ± 15 pc
D	811 ± 48 kpc	829 ± 42 kpc
$(m-M)_0$	24.55 ± 0.13	24.59 ± 0.11
$r_{\rm M31}$[b]	385^{+18}_{-13} kpc	198^{+18}_{-10} kpc
M_V	-8.7 ± 0.4	-8.5 ± 0.3
$\langle$[Fe/H]$\rangle$	-1.84 ± 0.15	-1.90 ± 0.12
σ([Fe/H])	0.65 ± 0.15	0.57 ± 0.11
HI	$<2.8 \times 10^3\,M_\odot$	

Notes.
[a] Schlafly & Finkbeiner (2011).
[b] 3D distance, rather than projected.

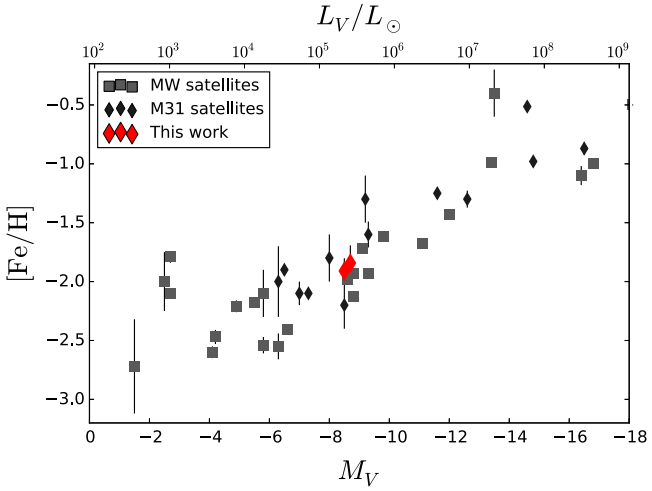

Figure 6. Luminosity–metallicity relation for Local Group satellites, adapted from the compilation presented in Ho et al. (2015), which includes data from Kirby et al. (2011) and Collins et al. (2013). Squares are MW satellites, diamonds are M31 satellites, and the error bars are from the Monte Carlo resampling of the [Fe/H] distribution for each galaxy. And XXVIII and XXIX are shown as the larger red diamonds. This demonstrates that And XXVIII and XXIX lie on the same metallicity–luminosity relation as other Local Group satellites.

and the posterior probability distributions for the half-light radius confirm the statistical significance of the difference. This behavior has been seen in other dwarf galaxies, such as Sculptor (Tolstoy et al. 2004), Fornax (Battaglia et al. 2006), Canes Venatici I (Ibata et al. 2006), And II (McConnachie et al. 2007), and Leo T (de Jong et al. 2008). In all of these cases the more metal-rich population is the more centrally concentrated one, consistent with And XXVIII. Measuring the spatial structure of the two components independently shows that they appear to be simply scaled versions of each other; the half-light radii are 370 ± 60 pc and 240 ± 15 pc (blue and red, respectively), while the ellipticities of 0.48 ± 0.06 and 0.43 ± 0.03, along with position angles of $45° \pm 5°$ and $34° \pm 3°$, agree well with each other. Taken together this implies that the

Table 2
Metallicities of And XXVIII and XXIX Stars

Galaxy	R.A. (deg)	Decl. (deg)	r_0	$(r-i)_0$	[Fe/H]	$\sigma_{[Fe/H]}$[a]
And XXVIII	338.16549	31.20840	21.397	0.53	−2.29	0.5
And XXVIII	338.18538	31.22404	21.404	0.44	−1.58	0.5
And XXVIII	338.15561	31.18421	21.381	0.45	−1.54	0.8
And XXVIII	338.14847	31.15615	21.001	0.24	−0.50	0.8
And XXVIII	338.17702	31.21802	21.548	0.42	−2.06	0.5
And XXVIII	338.17499	31.22058	21.969	0.35	−2.91	0.7
And XXVIII	338.18206	31.21668	21.509	0.41	−2.74	0.4
And XXVIII	338.16849	31.22444	22.344	0.42	−1.90	0.6
And XXVIII	338.18357	31.21526	21.332	0.38	−1.81	0.4
And XXVIII	338.17542	31.23720	21.57	0.70	−1.28	0.3
And XXVIII	338.15091	31.20916	21.578	0.46	−1.68	0.2
And XXVIII	338.18428	31.23235	21.861	0.37	−1.15	0.3
And XXVIII	338.22622	31.21862	21.78	0.37	−2.57	0.2
And XXIX	359.73912	30.74974	22.113	0.36	−1.83	0.5
And XXIX	359.72546	30.74484	21.467	0.45	−1.94	0.3
And XXIX	359.72690	30.76834	21.592	0.44	−1.29	0.4
And XXIX	359.74259	30.75986	22.084	0.42	−0.62	0.5
And XXIX	359.74561	30.75100	21.854	0.39	−2.40	0.4
And XXIX	359.71503	30.74976	21.369	0.40	−2.54	0.3
And XXIX	359.71755	30.74150	21.968	0.37	−3.14	0.5
And XXIX	359.71880	30.73644	22.003	0.40	−1.36	0.4
And XXIX	359.71957	30.76735	22.211	0.35	−1.86	0.6
And XXIX	359.75409	30.76225	21.172	0.45	−1.97	0.3
And XXIX	359.75959	30.76464	22.111	0.36	−1.77	0.6
And XXIX	359.73776	30.80015	21.266	0.20	−2.31	0.3
And XXIX	359.73609	30.79734	22.137	0.33	−1.68	0.5
And XXIX	359.68681	30.72895	21.959	0.36	−2.68	0.6
And XXIX	359.74074	30.76867	21.407	0.44	−1.89	0.4
And XXIX	359.74687	30.76948	21.751	0.29	−1.47	0.5
And XXIX	359.75467	30.75391	21.752	0.37	−1.63	0.5

Note.
[a] Individual star [Fe/H] uncertainity; not to be confused with the overall metallicity spread in Table 1.

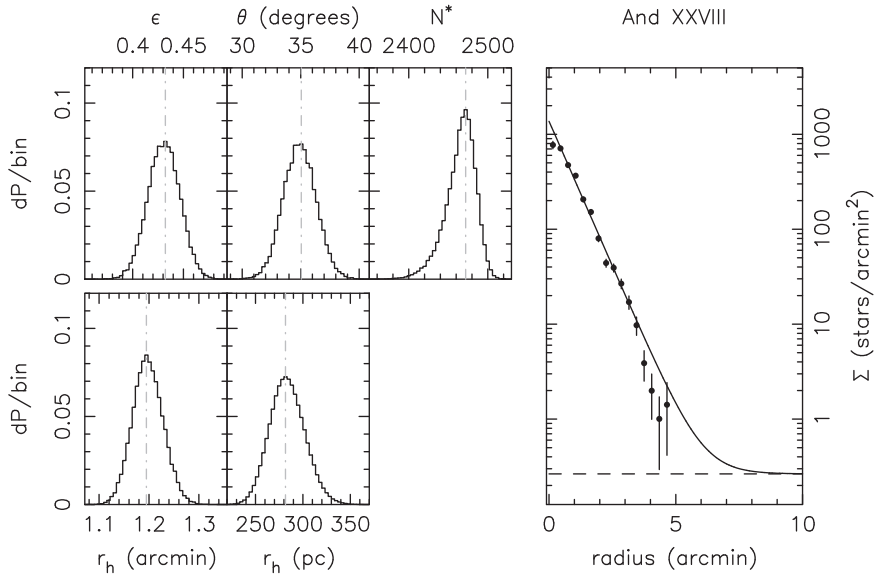

Figure 7. Posterior probability distributions for the structural parameters fit for And XXVIII are shown on the left. From top-left to bottom-right, these correspond to the ellipticity (ϵ), the position angle from north to east (θ), the number of stars under the profile for the assumed depth limit (N^*), the angular major-axis half-light radius (r_h), and its corresponding physical length assuming the distance modulus measured above. The radial profile is shown on the right, with the best fit exponential profile shown by the solid line and the dashed line showing the background level.

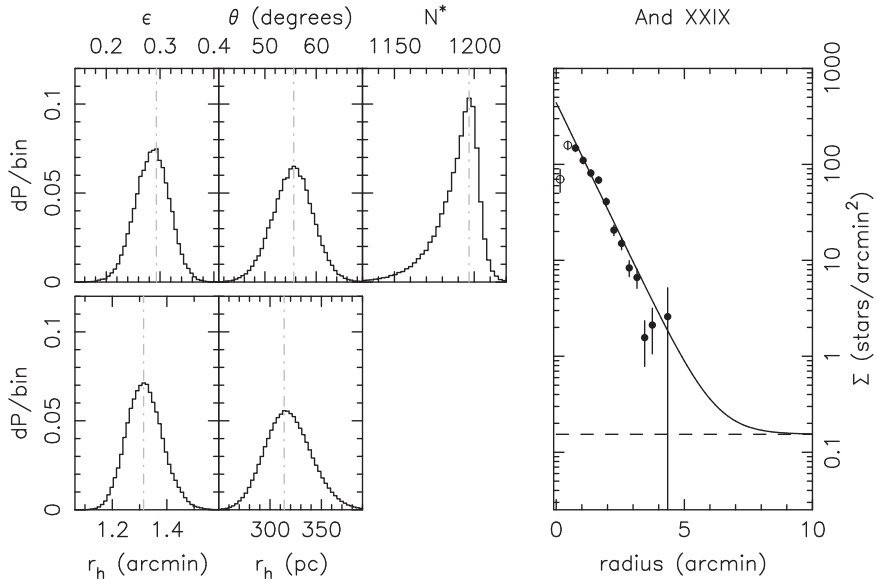

Figure 8. Same posterior probability distributions and radial profile as in Figure 7, but for And XXIX. The two innermost radial profile points (open circles) were not used in the fit due to the bright contamination in the center of the galaxy.

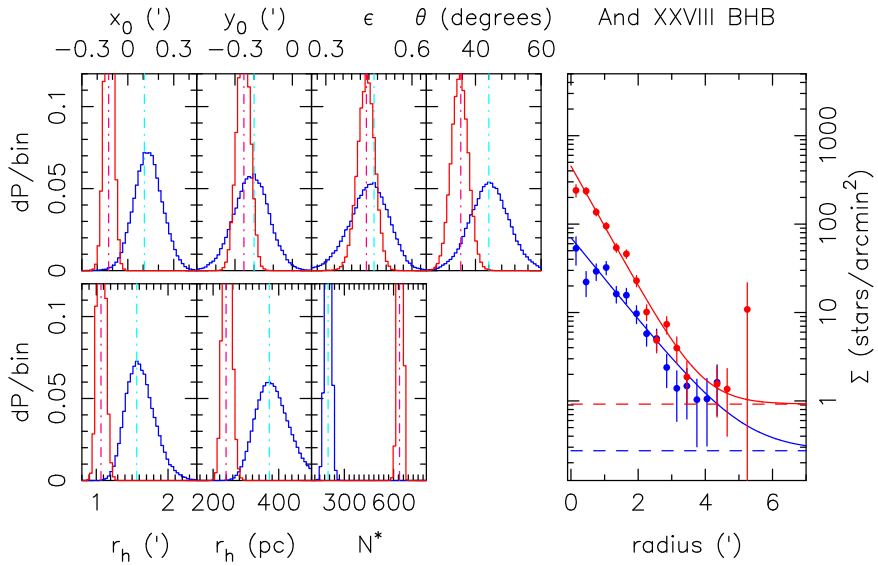

Figure 9. Posterior probability distributions for the structural fit of And XXVIII, performed separately for stars in the RHB (red lines) and the BHB (blue lines). The difference in the radial profile is clearly visible in the panel on the right, and the significance is confirmed by the difference in half light radius (r_h). The ellipticities and position angles are similar in the two populations.

process that transformed the dwarf into a pressure-supported system did so without randomizing the orbital energies of individual stars enough to completely redistribute the older and younger populations, but both populations did end up with the same general morphology.

Simulations of isolated dwarfs by Kawata et al. (2006) are able to reproduce a radial metallicity gradient, but with some uncertainty over the number of stars at the lowest metallicity values and the total luminosity of the simulated dwarfs (and also see Revaz & Jablonka (2012) for simulated dwarfs without gradients). In these simulations the metallicity gradient is produced by the continuous accretion of gas to the center of the galaxy, which tends to cause more metal enrichment and a younger population (weighted by mass) at small radii when compared to the outer regions of the galaxy. This explanation suggests that the "two populations" we infer from the RHB and BHB of And XXVIII are perhaps more properly interpreted as two distinct tracers of what is really a continuous range of ages and metallicities present in the dwarf. In this scenario, the lack of observed multiple populations in And XXIX could be the result of the dwarf lacking sufficient gas accretion and star formation activity to generate a strong metallicity gradient. If this is the case, then there may be a mass dependence to the presence of such gradients, which makes it particularly significant that And XXVIII is a relatively low-mass galaxy to host such a behavior. Whether this is merely stochasticity, or the influence of external forces, or if it requires a more complex model of the enrichment process is an open question.

6. DISCUSSION AND CONCLUSIONS

The analysis of And XXVIII and XXIX shows that both galaxies are relatively typical dwarf spheroidals, with old, metal-poor stellar populations and no measurable ongoing or recent star formation. The significance of these galaxies in distinguishing models of dSph formation comes from their considerable distances from M31. If environment-independent processes such as supernova feedback or reionization are responsible for transforming dIrrs into dSphs, then finding dSphs at these distances is quite natural. However, such models are by themselves largely unable to reproduce the radial dependence of the dSph distribution around the Milky Way and M31. An environment-based transformation process, based on some combination of tidal or ram pressure forces, can potentially account for the radial distribution, but correctly reproducing the properties of dSphs large radii is the critical test of such models. It is in this light that Andromeda XXVIII and Andromeda XXIX have the most power to discriminate between models.

Models of tidal transformation have been studied extensively and can account for many of the observed structural properties of dSphs (Mayer et al. 2001; Łokas et al. 2010, 2012). However, a critical component of understanding whether these models can reproduce the entire population of Local Group dSphs is the dependence of the transformation process on orbital pericenter distances and the number of pericentric passages. At large radii the weaker tidal force may lose its ability completely transform satellites into dSphs, potentially leaving observable signatures in satellites on the outskirts of host galaxies.

Observationally we cannot directly know the orbital history of individual satellites without proper motions (of which there are very few), and must test the radial distribution of dSphs in a statistical way. Slater & Bell (2013) used the Via Lactea simulations to show that a significant fraction of the dwarf galaxies located between 300 and 1000 kpc from their host galaxy have made at least one pericentric passage near a larger galaxy. However, the fraction of dwarfs that have undergone two or more pericentric passages decreases sharply near 300 kpc. This suggests that it is unlikely for And XXVIII to have undergone multiple pericentric passages.

This presents a clear question for theories of dSph formation based on tidal interactions: can a dwarf galaxy be completely transformed into a dSph with only a single pericenter passage? Simulations of tidal stirring originally seemed to indicate that the answer was no, and when dwarfs were placed on different orbits it was only the ones with several (~4–5) pericenter passages that were transformed into dSphs (Kazantzidis et al. 2011a). However, more recent simulations that used cored dark matter profiles for the dwarfs suggest that multiple pericenter passages might not be required. Kazantzidis et al. (2013) show that dwarfs with very flat central dark matter profiles (inner power-law slopes of 0.2) can be transformed into pressure supported systems after only one or two pericenter passages. This result is encouraging, but it also comes with the consequence that cored dark matter profiles also tend to make the dwarfs susceptible to complete destruction by tidal forces. In the simulations of Kazantzidis et al. (2013), five out of the seven dwarfs that were successfully transformed into dSphs after only one or two pericenter passages were subsequently destroyed. Taken together, these results indicate that rapid formation of a dSph is indeed plausible, but there may only be a narrow range of structural and orbital parameters compatible with such a process. Recent proper motion measurements of the dSph Leo I support this picture even further, as it appears to have had only one pericentric passage (Sohn et al. 2013) yet is unambiguously a dSph.

The properties of And XXVIII add an additional constraint that any tidal transformation must not have been so strong as to completely mix the older and younger stellar populations. A simple test case of this problem has been explored by Łokas et al. (2012), in which particles were divided into two populations by their initial position inside or outside of the half light radius. The dwarfs were then placed on reasonable orbits around a host galaxy, and evolved for 10 Gyr. The resulting radial profiles of the two populations are distinct in nearly all cases, with some variation depending on the initial conditions of the orbit. These tests may be overly optimistic, since initial differentiation into two populations is performed by such a sharp radius cut, but the simulations illustrate the plausibility of a dwarf retaining spatially distinct populations after tidal stirring.

An additional piece of the puzzle is provided by the metallicities. And XXVIII and XXIX are both consistent with the luminosity–metallicity relation shown by other Local Group satellites (see Section 4). This implies that they could not have been subject to substantial tidal *stripping*, as this would drive them off this relation by lowering the luminosity without substantially altering their metallicities. This point is further reinforced by the similarity of the luminosity–metallicity relation of both dSph and dIrr galaxies in the Local Group (Kirby et al. 2013), making it unlikely that the measured luminosity–metallicity relation itself is significantly altered by tidal stripping. Whether or not more gentle tidal effects can induce morphological transformation without altering the luminosity–metallicity relation remains to be seen.

Taken together, the properties of And XXVIII and XXIX present a range of challenges for detailed models of dwarf galaxy evolution to explain. Particularly for And XXVIII, the wide separation and low mass of the system add significant challenges to reproducing the gas-free spheroidal morphology with a stellar population gradient, while there may be similar challenges for explaining the apparent absence (or at least low-detectability) of such gradients in And XXIX. Though plausible explanations have been shown to exist for many of these features individually and under ideal conditions, whether the combination of these conditions can be accurately reproduced in a simulation is unknown. Further modeling of these types of systems is required before we can understand the physical drivers of these observed features.

We thank the anonymous referee for helpful comments which improved the paper. This work was partially supported by NSF grant AST 1008342. Support for E.J.T. was provided by NASA through Hubble Fellowship grant #51316.01 awarded by the Space Telescope Science Institute, which is operated by the Association of Universities for Research in Astronomy, Inc., for NASA, under contract NAS 5-26555. Based on observations obtained at the Gemini Observatory, which is operated by the Association of Universities for Research in Astronomy, Inc., under a cooperative agreement with the NSF on behalf of the Gemini partnership: the National Science Foundation (United States), the National Research Council (Canada), CONICYT (Chile), the Australian Research

Council (Australia), Ministério da Ciência, Tecnologia e Inovação (Brazil) and Ministerio de Ciencia, Tecnología e Innovación Productiva (Argentina). Some of the data presented herein were obtained at the W. M. Keck Observatory, which is operated as a scientific partnership among the California Institute of Technology, the University of California and the National Aeronautics and Space Administration. The Observatory was made possible by the generous financial support of the W. M. Keck Foundation. The authors wish to recognize and acknowledge the very significant cultural role and reverence that the summit of Mauna Kea has always had within the indigenous Hawaiian community. We are most fortunate to have the opportunity to conduct observations from this mountain.

Facility: Gemini:Gillett (GMOS), Keck:II (DEIMOS).

REFERENCES

Ahn, C. P., Alexandroff, R., Allende Prieto, C., et al. 2012, ApJS, 203, 21
An, D., Johnson, J. A., Clem, J. L., et al. 2008, ApJS, 179, 326
Battaglia, G., Tolstoy, E., Helmi, A., et al. 2006, A&A, 459, 423
Bell, E. F., Slater, C. T., & Martin, N. F. 2011, ApJL, 742, L15
Blitz, L., & Robishaw, T. 2000, ApJ, 541, 675
Brasseur, C. M., Martin, N. F., Macciò, A. V., Rix, H.-W., & Kang, X. 2011, ApJ, 743, 179
Carrera, R., Pancino, E., Gallart, C., & del Pino, A. 2013, MNRAS, 434, 1681
Chen, Y. Q., Zhao, G., & Zhao, J. K. 2009, ApJ, 702, 1336
Collins, M. L. M., Chapman, S. C., Rich, R. M., et al. 2013, ApJ, 768, 172
Conn, A. R., Lewis, G. F., Ibata, R. A., et al. 2013, ApJ, 766, 120
de Jong, J. T. A., Harris, J., Coleman, M. G., et al. 2008, ApJ, 680, 1112
Dekel, A., & Silk, J. 1986, ApJ, 303, 39
D'Onghia, E., Besla, G., Cox, T. J., & Hernquist, L. 2009, Natur, 460, 605
Dotter, A., Chaboyer, B., Jevremović, D., et al. 2008, ApJS, 178, 89
Einasto, J., Saar, E., Kaasik, A., & Chernin, A. D. 1974, Natur, 252, 111
Gnedin, N. Y. 2000, ApJ, 542, 535
Gnedin, O. Y., & Zhao, H. 2002, MNRAS, 333, 299
Grcevich, J., & Putman, M. E. 2009, ApJ, 696, 385
Grebel, E. K., Gallagher, J. S., III, & Harbeck, D. 2003, AJ, 125, 1926
Ho, N., Geha, M., Tollerud, E. J., et al. 2015, ApJ, 798, 77
Ibata, R., Chapman, S., Irwin, M., Lewis, G., & Martin, N. 2006, MNRAS, 373, L70
Ibata, R. A., Lewis, G. F., Conn, A. R., et al. 2013, Natur, 493, 62
Kawata, D., Arimoto, N., Cen, R., & Gibson, B. K. 2006, ApJ, 641, 785
Kazantzidis, S., Łokas, E. L., Callegari, S., Mayer, L., & Moustakas, L. A. 2011a, ApJ, 726, 98
Kazantzidis, S., Łokas, E. L., & Mayer, L. 2013, ApJL, 764, L29
Kazantzidis, S., Łokas, E. L., Mayer, L., Knebe, A., & Klimentowski, J. 2011b, ApJL, 740, L24
Kirby, E. N., Cohen, J. G., Guhathakurta, P., et al. 2013, arXiv:1310.0814
Kirby, E. N., Lanfranchi, G. A., Simon, J. D., Cohen, J. G., & Guhathakurta, P. 2011, ApJ, 727, 78
Klimentowski, J., Łokas, E. L., Kazantzidis, S., Mayer, L., & Mamon, G. A. 2009, MNRAS, 397, 2015
Kravtsov, A. V., Gnedin, O. Y., & Klypin, A. A. 2004, ApJ, 609, 482
Łokas, E. L., Kowalczyk, K., & Kazantzidis, S. 2012, arXiv:1212.0682
Łokas, E. L., Kazantzidis, S., Klimentowski, J., Mayer, L., & Callegari, S. 2010, ApJ, 708, 1032
Mac Low, M.-M., & Ferrara, A. 1999, ApJ, 513, 142
Martin, N. F., de Jong, J. T. A., & Rix, H.-W. 2008, ApJ, 684, 1075
Mayer, L., Governato, F., Colpi, M., et al. 2001, ApJ, 559, 754
Mayer, L., Mastropietro, C., Wadsley, J., Stadel, J., & Moore, B. 2006, MNRAS, 369, 1021
McConnachie, A. W., Peñarrubia, J., & Navarro, J. F. 2007, MNRAS, 380, L75
Muñoz, R. R., Padmanabhan, N., & Geha, M. 2012, ApJ, 745, 127
Revaz, Y., & Jablonka, P. 2012, A&A, 538, AA82
Ryan-Weber, E. V., Begum, A., Oosterloo, T., et al. 2008, MNRAS, 384, 535
Sarajedini, A., Lee, Y.-W., & Lee, D.-H. 1995, ApJ, 450, 712
Sawala, T., Scannapieco, C., Maio, U., & White, S. 2010, MNRAS, 402, 1599
Ségall, M., Ibata, R. A., Irwin, M. J., Martin, N. F., & Chapman, S. 2007, MNRAS, 375, 831
Schlafly, E. F., & Finkbeiner, D. P. 2011, ApJ, 737, 103
Slater, C. T., & Bell, E. F. 2013, arXiv:1306.1829
Slater, C. T., Bell, E. F., & Martin, N. F. 2011, ApJL, 742, L14
Sohn, S. T., Besla, G., van der Marel, R. P., et al. 2013, ApJ, 768, 139
Stetson, P. B. 1987, PASP, 99, 191
Stetson, P. B., Hesser, J. E., Smith, G. H., Vandenberg, D. A., & Bolte, M. 1989, AJ, 97, 1360
Teyssier, M., Johnston, K. V., & Kuhlen, M. 2012, MNRAS, 426, 1808
Tollerud, E. J., Geha, M. C., Vargas, L. C., & Bullock, J. S. 2013, ApJ, 768, 50
Tolstoy, E., Irwin, M. J., Helmi, A., et al. 2004, ApJL, 617, L119
van den Bergh, S. 1994, ApJ, 428, 617